

# Spatio-temporal filtering properties of a dendritic cable with active spines: a modeling study in the spike-diffuse-spike framework

Y Timofeeva (yulia@ma.hw.ac.uk) and G J Lord  
(gabriel@ma.hw.ac.uk)

*Department of Mathematics, Heriot-Watt University, Edinburgh, EH14 4AS, UK.*

S Coombes (stephen.coombes@nottingham.ac.uk)

*School of Mathematical Sciences, University of Nottingham, Nottingham, NG7 2RD, UK.*

## Abstract.

The spike-diffuse-spike (SDS) model describes a passive dendritic tree with active dendritic spines. Spine-head dynamics is modeled with a simple integrate-and-fire process, whilst communication between spines is mediated by the cable equation. In this paper we develop a computational framework that allows the study of multiple spiking events in a network of such spines embedded on a simple one-dimensional cable. In the first instance this system is shown to support saltatory waves with the same qualitative features as those observed in a model with Hodgkin-Huxley kinetics in the spine-head. Moreover, there is excellent agreement with the analytically calculated speed for a solitary saltatory pulse. Upon driving the system with time-varying external input we find that the distribution of spines can play a crucial role in determining spatio-temporal filtering properties. In particular, the SDS model in response to periodic pulse train shows a positive correlation between spine density and low-pass temporal filtering that is consistent with the experimental results of Rose and Fortune [1999, ‘Mechanisms for generating temporal filters in the electrosensory system’. *The Journal of Experimental Biology* **202**, 1281–1289]. Further, we demonstrate the robustness of observed wave properties to natural sources of noise that arise both in the cable and the spine-head, and highlight the possibility of purely noise induced waves and coherent oscillations.

**Keywords:** spike-diffuse-spike, dendritic spines, filtering, noise

## 1. Introduction

In 1891 Ramón y Cajal showed that dendritic spines are present in the dendrites of many neurons of the cerebral cortex of mammals (Cajal, 1891). Dendritic spines are small mushroom like appendages with a bulbous head and a tenuous stem (of length around  $1\mu\text{m}$ ) and may be found in their hundreds of thousands on the dendritic tree of a single cortical pyramidal cell. These extensions of the dendritic tree provide junction points for the axons of other neurons (i.e., provide surface area for synapses), and thus serve as loci for receiving inputs.



© 2005 Kluwer Academic Publishers. Printed in the Netherlands.

In the cerebral cortex approximately 80% of all excitatory synapses are made onto dendritic spines. Since the biophysical properties of spines can be modified by experience in response to patterns of chemical and electrical activity, morphological and electro-chemical changes in populations of dendritic spines are thought to provide a basic mechanism for Hebbian learning in the nervous system. In fact as far back as 1899 Cajal (1899) was arguing that spines could be involved in learning and that physical changes in spines were associated with neuronal function, suggesting that they might grow with activity and retract during inactivity or sleep. These notions continue to be influential in the study of the function of dendritic spines even today (Yuste and Bonhoeffer, 2001; Yuste and Majewska, 2001).

In recent years the properties of spines have also been linked with the implementation of logical computations (Shepherd and Brayton, 1987) coincidence detection (Larkum et al., 1999) orientation tuning in complex cells of visual cortex (Mel et al., 1998) and the amplification of distal synaptic inputs (Miller et al., 1985). At the organismal level there is now evidence to suggest that the density of dendritic spines may reflect overall mental agility (Zito and Murthy, 2002). Conversely, many neurological diseases resulting in mental retardation have been associated with spine loss or spine morphology changes (such as Fragile X-syndrome<sup>1</sup>). However, the focus of this paper will be on the implication of excitable channels in the spine-head membrane for single neuron dynamics. The benefits of excitable membrane for the amplification of excitatory synaptic inputs was first discussed by Jack et. al. (1975). If dendritic spines possess excitable membrane, the spread of current from one spine along the dendrites may bring adjacent spines to threshold for impulse generation, resulting in a saltatory propagating wave in the distal dendritic branches (Shepherd et al., 1985). However, it is only relatively recently that confocal and two-photon microscopy observations have confirmed the generation of action potentials in the dendrites (see (Segev and Rall, 1998) for a perspective).

The first step towards the development of a spiny dendritic tissue model that might be used to explore these issues can be attributed to Baer and Rinzel (1991) who considered a passive uniform unbranched dendritic tree coupled to a population of excitable dendritic spines. In this *continuum* model the active spine-head dynamics is modeled with Hodgkin-Huxley (HH) kinetics whilst the (distal) dendritic tissue is modeled with the cable equation. The spine-head is coupled to the cable via a spine-stem resistance that delivers a current proportional to the number of spines at the contact point. There is no direct coupling

---

<sup>1</sup> <http://www.fraxa.org/>

between neighboring spines; voltage spread by diffusion along the cable is the only way for spines to interact. Although the numerical studies of Baer and Rinzel (1991) show traveling wave solutions, the underlying continuous nature of the model precludes the possibility that these waves are truly saltatory. The saltatory nature of a propagating wave in a spiny neuron may be directly attributed to the fact that active spines are physically separated. Although we can numerically simulate the nonlinear and nonuniform properties of biologically realistic dendritic trees with discrete and clustered distributions of spines, based around natural extensions of the Baer-Rinzel (BR) model, there is a lack of analytical tools for dealing with such systems. However, recent work by Coombes, Bressloff and Lord (Coombes and Bressloff, 2000; Coombes, 2001b; Lord and Coombes, 2002; Coombes and Bressloff, 2003) has shown that the active membrane dynamics of spines can be treated using an analytically tractable integrate-and-fire (IF) process. The resulting model has been termed the Spike-Diffuse-Spike (SDS) model since spine-head dynamics is an all-or-nothing action potential response, whilst the dendritic cable is modeled as a passive structure. Not only can saltatory wave propagation be naturally analyzed in the SDS framework, the model is computationally inexpensive and ideally suited for the study of neural response to complicated spatio-temporal patterns of synaptic input that typically occur in cortical neurons. It is precisely these points we choose to highlight in this paper.

In section 2 we review the SDS framework and extend previous work by showing how one may express solutions in terms of a Dyson-like series expansion. Moreover, we discuss the numerical implementation of analytical solutions to the SDS model that depend upon numerically determined firing events. For comparison with more conventional (numerical PDE) approaches we also develop an implementation of the SDS model within the NEURON simulation environment (Hines and Carnevale, 2003). As a first illustration of the usefulness of the SDS model of spiny dendritic tissue we present a case study of saltatory propagating waves in a model with regularly spaced spines. Also in section 3 we treat wave propagation (and its failure) for more irregular distributions of spines. After establishing the ability of the SDS model to accurately describe the sorts of saltatory waves one finds in the more biophysically detailed BR model, we turn next, in section 4, to the issue of the active dendritic tree as a nonlinear filter. In particular we use the SDS model to address the observation of Rose and Fortune (1999) that there is a positive correlation between spine density and low-pass temporal filtering. In section 5 we test the robustness of observed wave and filtering properties to natural sources of noise that arise both in the cable and the spine-head, and highlight the possibility of purely

noise induced waves and coherent oscillations. Finally, in section 6, we look forward and describe some of the open problems in single neuron function that may be readily addressed with a further analysis of SDS dynamics.

## 2. The spike-diffuse-spike model

We consider a uniform passive dendritic cable with a given distribution of spines along its length. A schematic diagram of the SDS model is shown in Figure 1. The dynamics of membrane voltage in the cable

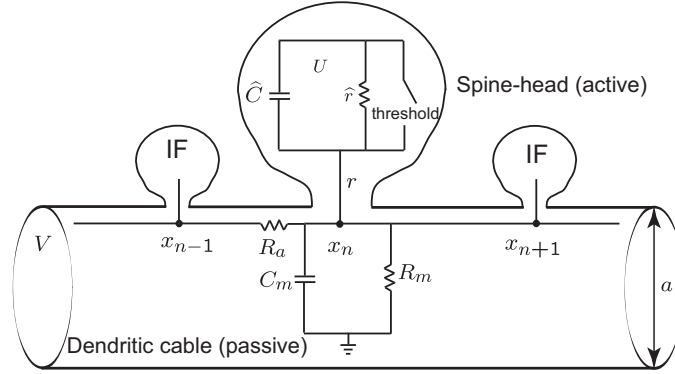


Figure 1. A schematic representation of the SDS model showing a passive cable with electrically connected active spines.

$V = V(x, t)$  is described by the equation

$$\pi a C_m \frac{\partial V}{\partial t} = \frac{\pi a^2}{4 R_a} \frac{\partial^2 V}{\partial x^2} - \frac{\pi a}{R_m} V + \rho(x) I_{sp}. \quad (1)$$

Here  $a$  is a diameter of the cable (measured in  $\mu\text{m}$ ),  $R_a$  is the specific cytoplasmic resistivity (in  $\Omega \cdot \text{cm}$ ),  $C_m$  and  $R_m$  are respectively the specific membrane capacity (in  $\mu\text{F}/\text{cm}^2$ ) and a resistance across a unit area of passive membrane (in  $\Omega \cdot \text{cm}^2$ ). Spines are connected to the cable at the discrete points  $x_n$  with the distribution function  $\rho(x) = \sum_{n \in \Gamma} \delta(x - x_n)$ , where  $\Gamma$  is a discrete set that indexes the spines. Each spine generates a sequence of action potentials in its spine-head given by the function  $\hat{V}(x, t)$ . As a result the spine that just “fired” passes the spine current  $I_{sp} = (\hat{V} - V)/r$  into the cable. The spine stem resistance of an individual spine is given by  $r$ . Denoting  $T_n^m$ ,  $m \in \mathbb{Z}$  as the time of the  $m$ th firing event of the  $n$ th spine the function  $\hat{V}(x_n, t)$  is given by  $\hat{V}(x_n, t) = \sum_m \eta(t - T_n^m)$ . Here  $\eta(t)$  specifies the universal

shape of an action potential. The generator of action potentials in the  $n$ th spine-head evolves according to

$$\hat{C} \frac{\partial U_n}{\partial t} = -\frac{U_n}{\hat{r}} + \frac{V_n - U_n}{r} - \underbrace{\hat{C} h \sum_m \delta(t - T_n^m)}_{\text{reset}}, \quad (2)$$

where  $V_n = V(x_n, t)$ . Here the parameters  $\hat{C}$  and  $\hat{r}$  describe the electrical properties of the spine-head membrane, namely its capacitance and resistance respectively. The spine's firing times  $T_n^m$  are defined in terms of the IF process according to

$$T_n^m = \inf\{t \mid U_n(t) \geq h, t > T_n^{m-1} + \tau_R\}. \quad (3)$$

Hence, a spine fires whenever  $U_n$ , driven by current from the shaft, crosses some threshold potential  $h$ . Just after the firing event the variable  $U_n$  resets to zero, modeled by the last term in equation (2). Multiple spiking events from an individual spine are controlled by a refractory time-scale  $\tau_R$  during which the spine can not fire.

It is convenient to rewrite (1) in the standard form

$$\frac{\partial V}{\partial t} = D \frac{\partial^2 V}{\partial x^2} - \frac{V}{\tau} + Dr_a \rho(x) \frac{\hat{V} - V}{r}, \quad (4)$$

where  $D = \lambda^2/\tau$  denotes the diffusion coefficient of the cable,  $\tau = C_m R_m$  is the membrane time constant,  $\lambda = \sqrt{a R_m / 4 R_a}$  is the electronic space constant and  $r_a = 4 R_a / \pi a^2$  denotes the intracellular resistance per unit length of cable. The integration of this equation gives us an implicit expression for the membrane potential in the form

$$V(x, t) = \frac{Dr_a}{r} \sum_{k \in \Gamma} \int_0^t ds G(x - x_k, t - s) [\hat{V}(x_k, s) - V(x_k, s)]. \quad (5)$$

Here,  $G(x, t)$  is the Green's function of the infinite uniform passive cable

$$G(x, t) = \frac{1}{\sqrt{4\pi Dt}} e^{-\varepsilon t} e^{-x^2/(4Dt)} \Theta(t), \quad (6)$$

where  $\varepsilon = 1/\tau$  and  $\Theta(t)$  is the Heaviside step function. The expression for the cable voltage (5) has a Dyson-like form (Bressloff and Coombes, 1997) suggesting a Neumann series solution, obtained by repeated substitution of (5) into itself. Introducing the parameter  $\Lambda = Dr_a/r$ , and generating just the first two terms in this expansion gives

$$\begin{aligned} V(x, t) = & \Lambda \sum_k \int_0^t ds G(x - x_k, t - s) \hat{V}(x_k, s) \\ & - \Lambda^2 \sum_{k,p} \int_0^t ds G(x - x_k, t - s) \int_0^s ds' G(x_k - x_p, s - s') \hat{V}(x_p, s'), \end{aligned} \quad (7)$$

where  $\{p, k\} \in \Gamma$ . Under the approximation that  $\Lambda \ll 1$ , only the first term significantly contributes to the full solution. This first term is an exact solution of the SDS model in the presence of a partial current flux  $I_{\text{sp}} = \hat{V}/r$  from the spine-head into the cable instead of the original full flux. This gives rise to the so-called *partial SDS model*. In this case the solution takes the explicit form

$$V(x, t) = \Lambda \sum_{k \in \Gamma, m} H(x - x_k, t - T_k^m), \quad \max_{k, m} \{T_k^m\} \leq t < T_j^\ell, \quad (8)$$

where  $m = m(k)$  counts firing events at each spine and  $H(x, t) = \int_0^t G(x, t - s) \eta(s) ds$ . For a simple action potential shape given by a rectangular pulse  $\eta(t) = \eta_0 \Theta(t) \Theta(\tau_S - t)$  (with strength  $\eta_0$  and duration  $\tau_S$ ), the function  $H(x, t)$  can be found in closed form (Coombes and Bressloff, 2003) as  $H(x, t) = A_\varepsilon(x, t - \min(t, \tau_S)) - A_\varepsilon(x, t)$  with a standard integral  $A_\varepsilon(x, t)$  given in Appendix A. Equation (8) holds for times  $t$  between  $\max_{k, m} \{T_k^m\}$  (i.e., the last firing event from the set of all spine firing times), and  $T_j^\ell$  the time of the new firing event at the  $\ell$ th spine.

The firing times for the construction of solution (8) may be found from the set of threshold conditions  $U_n(t) = h$ , with  $U_n(t)$  obtained by integrating equation (2). In particular, to find a new firing time  $T_j^\ell > \max_{k, m} \{T_k^m\}$  corresponding to the spine at location  $x_j$  we have to solve the set of threshold conditions for the functions

$$U_n(t) = \frac{Dr_a}{\hat{C}r^2} \sum_{k, m} \hat{H}(x_n - x_k, t - T_k^m) - h \sum_m e^{-\varepsilon_0(t - T_n^m)}, \quad (9)$$

where

$$\hat{H}(x, t) = \int_0^t e^{\varepsilon_0(s-t)} H(x, s) ds, \quad (10)$$

and  $\varepsilon_0 = (1/\hat{r} + 1/r)/\hat{C}$ . For  $\varepsilon > \varepsilon_0$  this integral can be found in closed form as  $\hat{H}(x, t) = (A_\varepsilon(x, 0)(e^{-\varepsilon_0(t - \min(t, \tau_S))} - e^{-\varepsilon_0 t}) + \hat{A}(x, t - \min(t, \tau_S)) - \hat{A}(x, t))/\varepsilon_0$  with

$$\hat{A}(x, t) = e^{-\varepsilon_0 t} [A_{\varepsilon - \varepsilon_0}(x, 0) - A_\varepsilon(x, 0) - A_{\varepsilon - \varepsilon_0}(x, t)] + A_\varepsilon(x, t). \quad (11)$$

Alternatively the integral in (10) can be readily evaluated numerically for the explicitly given function  $H(x, t)$ .

By solving the set of threshold conditions with  $U_n(t)$  defined by (9) we obtain a vector of times showing when each spine is able to reach the threshold  $h$ . The smallest time from this vector,  $T_j^\ell$ , that satisfies the refractory restriction  $T_j^\ell - T_j^{\ell-1} > \tau_R$  defines a new spiking event at location  $x_j$ . The firing times of an individual spine have to be separated

by at least  $\tau_S$ , so the refractory time is restricted by  $\tau_R \geq \tau_S$ . As a result of finding the newly fired spine extra terms have to be added into both sums in (9). The same routine is then repeated to obtain subsequent firing events.

### 2.1. NUMERICAL IMPLEMENTATION OF THE SDS MODEL

The analytical integration of the equations of motion to get the explicit equations (8) and (9) for the partial SDS model obviates the need for the numerical solution of a partial differential equation. In the computations below we have taken  $\varepsilon > \varepsilon_0$  so that the explicit solution (10) and (11) can be used. Up to determining the firing times this gives us an analytic solution. The numerical scheme for the explicitly defined solution was implemented in MATLAB and the firing times (defined from the threshold conditions  $U_n(t) = h$ ) were determined numerically using the root-finding routine `fzero`. For each time interval the number of equations used for finding the earliest threshold crossing event can be reduced by excluding the spines that are still in the refractory state. Once the latest firing event has been determined then  $V(x, t)$  can be evaluated (in terms of a sum over all spines and all previous firing events). Since contributions from firing events in the distant past are exponentially decaying it would be safe to truncate this sum over events, and further improve numerical efficiency, though we do not do so in this paper.

In the following section we compare and validate the results from the (quasi) analytic solution of (10) and (11) detailed above. We show convergence by solving the explicit equation (7) for  $V(x, t)$  rather than (8) which requires the solution of the differential equation (2) for each spine. We also compare to the SDS model given as a system of differential equations implemented in NEURON (Hines and Carnevale, 2003). We solve the partial model with flux  $I_{sp} = \hat{V}/r$  from the spine-head into the cable as well as the full SDS model (1) and (2). We also compare to the BR model with discrete spines, again implemented in NEURON. All code is available upon request to the authors.

## 3. Validation of models and saltatory wave propagation

We validate the different models and their numerical solution by comparing the propagation of a solitary saltatory wave. We start by noting that for the (quasi) analytic case a solitary wave can be determined from the solution of a nonlinear algebraic equation.

Assume that the spines are regularly distributed along the cable with spacing  $d$ , i.e.,  $x_n = nd$ . The speed of a solitary wave propagating

in such a system may be determined in a self-consistent manner (see Coombes and Bressloff, 2003) by the implicit equation

$$h = \frac{\Lambda}{\widehat{C}r} \sum_{n=1}^{\infty} \widehat{H}(nd, n\Delta), \quad (12)$$

for the partial SDS model. Here  $\Delta$  measures the time between successive threshold crossings at adjacent spine-heads and thus, the speed is  $v = d/\Delta$ . In Figure 2 we plot this speed (solid curve) as a function of distance between the spines. If the spines are separated beyond some critical value (to the right of limit point LP) the wave fails to propagate. From the analysis in (Coombes, 2001a) it is further possible to establish that the faster of the two branches is stable. On the same figure we plot the results obtained from direct numerical simulations. In all simulations the wave is initiated from an activated single spine at one end of the cable (and free boundary conditions are assumed). Crosses indicate the speed obtained by using the explicit solution of the SDS model given by equations (8) and (9). Stars demonstrate the speed found by solving the system of differential equations. There is excellent agreement between both approaches as well as with the speed found from equation (12). Circles in Figure 2 denote the results of the full SDS model. The spine current passed into the cable in the full model is relatively less than in the partial model when other parameters are fixed. This explains why the wave in the last model propagates faster with the LP for propagation failure shifted to the right. If the firing events in the model are defined by using the full form of the solution for  $V(x, t)$  given by equation (5) the results will agree with the numerical solution of the full SDS model. To demonstrate this convergence of the explicit approach, we evaluate the speed of wave propagation using the explicit equation (7) for  $V(x, t)$  rather than (8). Equation (7) includes a second order term in  $\Lambda$  and this term has to be evaluated numerically. In this case the functions  $U_n(t)$  used for the determination of firing events are found by solving the differential equation (2) for each spine. The obtained speed of the wave is indicated by triangles in Figure 2. The inclusion of the second order term in the expansion for the full solution yields a slower wave speed (than with just the first order term). As more terms are included in the expansion the wave speed gets closer to the solution of the full model. The inner plot in this figure is a magnified view (for small lattice spacing), and demonstrates that the speed of the wave attains a maximum for small  $d$ . In Figure 5 we plot the voltage at the location of the 10th spine along the cable when  $d = 0.4$ . Here it is seen that the voltage of the fast wave in the partial SDS model has a higher amplitude compared to that of the full SDS model. However, even working to only second order in  $\Lambda$  yields



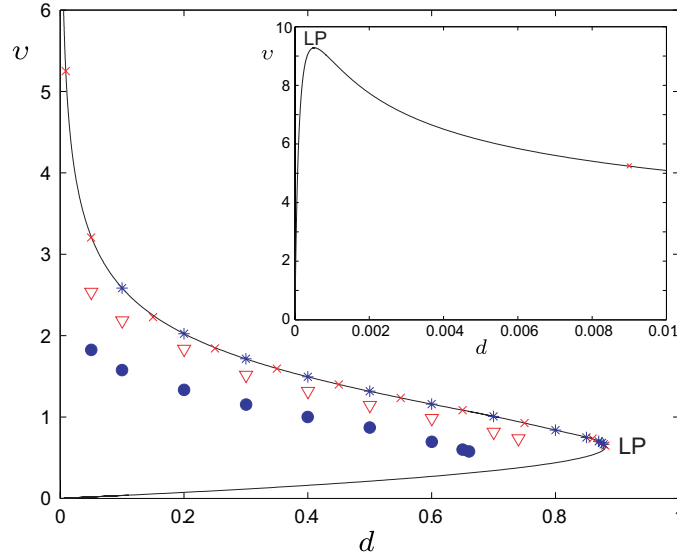


Figure 2. A plot of solitary wave speed  $v$  (in units  $\lambda/\tau$ ) as a function of the distance between the spines  $d$  (in units  $\lambda$ ). Solid line: the solution of equation (12). Crosses: the solution given by the explicit equations (8) and (9). Stars and circles: the solutions defined by solving (1) and (2) for the partial and full SDS model respectively. Triangles: the solution defined by solving (2) and (7). Parameters:  $D = 1$ ,  $\tau_S = \varepsilon = 1$ ,  $\eta_0 = 1$ ,  $\varepsilon_0 = 0.8$ ,  $\hat{C} = 2.5$ ,  $r = 1$ ,  $\tau_R = 10$ ,  $\hat{h} \equiv h/Dr_a = 0.05$ . Inner plot is a magnified view of a part of the speed curve showing the LP for  $v$ .

an improved solution, with increasing agreement as we include more terms in the series expansion for  $V(x, t)$ .

### 3.1. VALIDATION AGAINST THE BAER-RINZEL MODEL

The SDS model defined in terms of the IF process is a reduced version of the biophysically realistic model of Baer and Rinzel where the spine-head dynamics are modeled by HH kinetics. To compare these two models, we consider the BR model with a discrete distribution of spines rather than with the spines uniformly distributed along the cable (Baer and Rinzel, 1991, Lord and Coombes, 2002). In this case the model is defined by equation (1) and

$$\hat{C} \frac{\partial \hat{V}}{\partial t} = -I(\hat{V}, m, n, h) - \frac{\hat{V} - V}{r}. \quad (13)$$

Here the function  $I$  is the standard HH current, listed in Appendix B for completeness. The membrane current arises mainly through the conduction of sodium and potassium ions through voltage dependent

channels in the membrane. A numerical simulation of the BR model with a regular distribution of spines is presented in Figure 3 which shows a space-time density plot of  $V(x, t)$ . This plot nicely illustrates an example of a saltatory traveling wave solution.

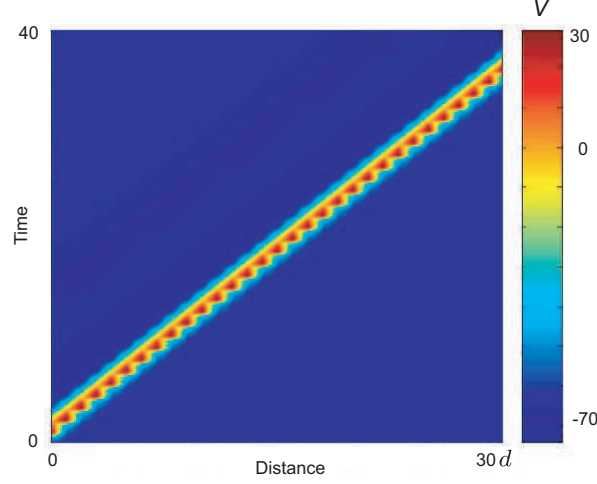


*Figure 3.* An example of saltatory traveling wave in the BR model with a discrete distribution of spines and spine spacing  $d = 5$ . Other parameters are given in Appendix B.

The speed of a saltatory wave changes when we vary the distance between the spines, and is quantified in Figure 4. Also in this figure we show a plot of the wave speed for the partial SDS model (solid curve), with parameters chosen so as to give a corresponding fit to the more biophysically detailed BR model.

From now on we consider the SDS model to be the (quasi) analytic solution of the partial SDS model obtained by solving equations (8) and (9) with a numerical approximation to the firing time.

### 3.2. SALTATORY WAVES AND SPINE DISTRIBUTIONS

Waves generated in the SDS model travel in a saltatory manner because the discreteness of the spine distribution breaks the translation symmetry of the underlying cable. An example of a saltatory wave (constructed from (10) and (11)) is shown in Figure 6. In Figure 7 we show a space-time plot of the cable voltage with 30 regularly distributed spines, which nicely illustrates (as does Figure 3) that although the wave has a saltatory nature it travels with well-defined speed. For

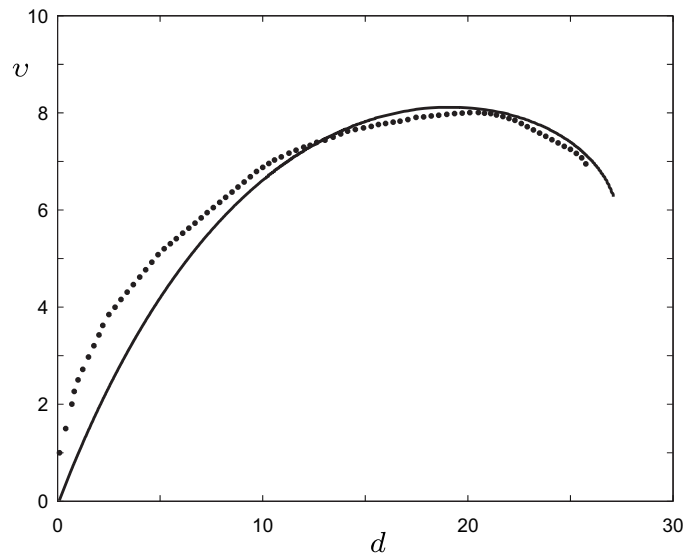


Figure 4. The speed of wave propagation  $v$  as a function of the distance between the spines  $d$  in the discrete BR model (dotted curve) and in the partial SDS model (solid curve). Parameters of the SDS model:  $D = 0.0003$  m/s,  $\eta_0 = 100$  mV,  $\tau_S = 2$  ms,  $r = 0.01$  M $\Omega$ ,  $\hat{C} = 0.001$   $\mu$ F,  $\varepsilon = 3$ ,  $\varepsilon_0 = 0.7$ ,  $\tilde{h} \equiv h/r_a = 0.00095$ . Parameters of the BR model are given in Appendix B.

sufficiently small values of the refractory period it is also possible to generate periodic traveling waves. An example is shown in Figure 8.

In real dendritic tissue the distribution of spines is likely to be irregular. In the SDS framework we might simply consider that the distribution function  $\rho(x)$  has some disorder. An example of the effect that such disorder can have is shown in Figure 9, where we choose spine positions from a uniform distribution. In comparison to Figure 7, not only does this cause irregular (and repeated) wave propagation, but it may lead to back-propagating waves. As expected, too much spatial disorder in the spine distribution can lead to propagation failure, when any one pair of adjacent spines becomes too far separated to cause firing of one by the other.

#### 4. Filtering properties

The spatio-temporal patterns of activity in neurons and indeed networks of neurons is intimately linked to the processing of sensory information. A fundamental issue in understanding the relationship between structure and function is how neurons transform and represent infor-

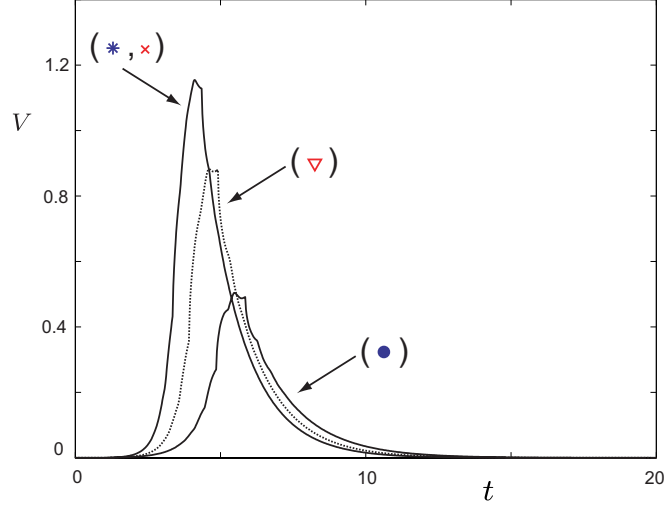


Figure 5. Voltage  $V$  (in units of  $\eta_0$ ) at the location of the 10th spine along the cable with spine spacing  $d = 0.4$ . Other parameters as in Figure 2. Left (right) solid curve: the solution of the partial (full) SDS model. Dashed curve: the solution of the full SDS model including terms up to order  $\Lambda^2$ .

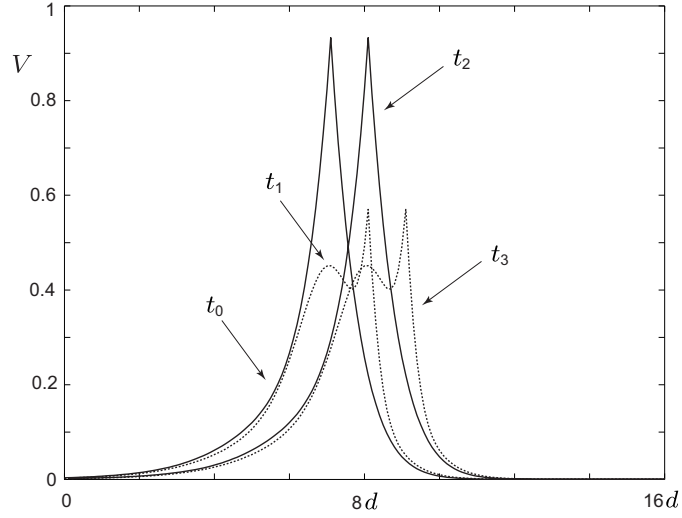


Figure 6. An example of saltatory solitary wave in the partial SDS model traveling along the cable with spine spacing  $d = 0.6$  and  $D = 0.25$ . Other parameters as in Figure 2. Snapshots are shown for times  $t_0 = 7\Delta + \tau_S$ ,  $t_1 = 8\Delta + 0.1\tau_S$ ,  $t_2 = 8\Delta + \tau_S$  and  $t_3 = 9\Delta + 0.1\tau_S$ , where  $\Delta = 1.1217$ .

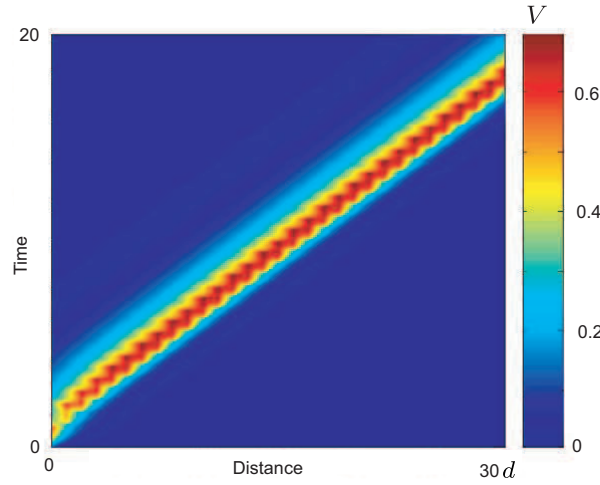


Figure 7. An example of saltatory traveling pulse in the partial SDS model initiated from a single active spine and moving out through the cable with 30 regularly spaced spines when  $d = 0.6$ . Other parameters as in Figure 2 except  $\tau_R = 6$ .

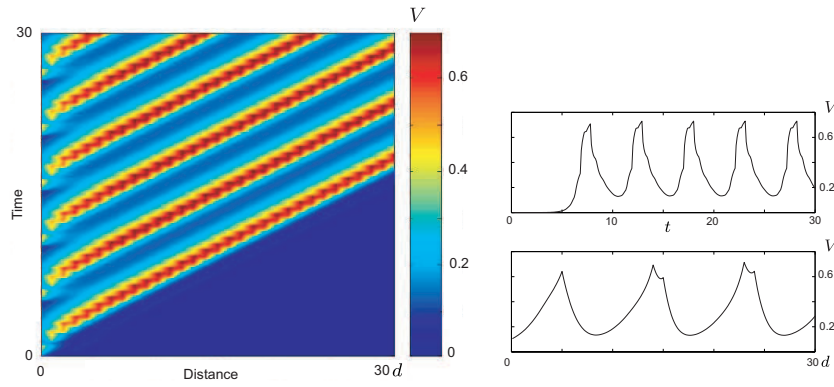


Figure 8. An example of periodic traveling wave for the model of Figure 7 with  $\tau_R = 5$ . Plots on the right illustrate the voltage potential as a function of time  $t$  at the location of the 10th spine along the cable (top plot) and as a function of space  $x$  at time  $t = 25$  (bottom plot).

mation using such patterns. In this regard an understanding of how neural systems respond to sensory stimuli is an important issue. Indeed, although the selective behavioral responses to stimuli in the sensory systems of many organisms is believed to rely on the presence of filters for the neural representations of the temporal structure of sensory signals, the mechanisms underlying this temporal selectivity are not

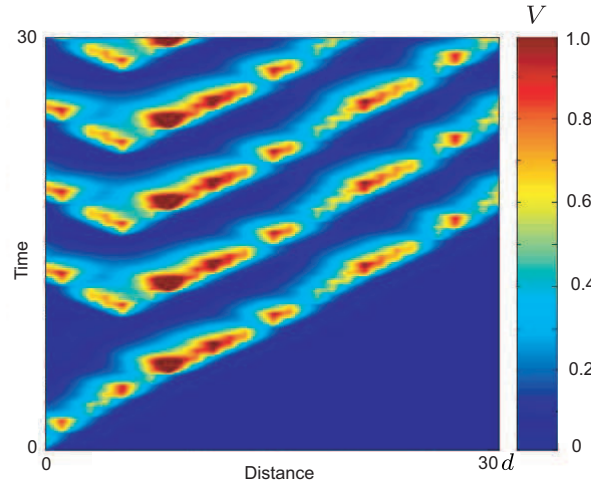


Figure 9. An example of irregular wave propagation in the partial SDS model for the parameter set corresponding to Figure 7 with 33 spine positions chosen from a uniform distribution.

completely understood. Undoubtedly these mechanisms are subserved by the biophysics of neurons, including the passive electrical properties of a neuron, and the types and distribution of channels and conductances they support. However, only relatively recently has a role for dendritic spines begun to be seriously entertained. For an increased understanding of the role of spines in temporal filtering, intracellular recordings are necessary. Progress in recording from neurons as small as  $10\text{ }\mu\text{m}$  has been made using ‘patch-type’ pipette techniques (Rose and Fortune, 1996), and these have been used to investigate the role of spines in filtering temporal input patterns to midbrain neurons of the weakly electric fish *Eigenmannia* (Fortune and Rose, 1997; Rose and Fortune, 1999). In particular, this work has shown that neurons with a broad dendritic arbor and relatively spiny dendrites demonstrate low-pass temporal filtering properties in response to input stimuli. Here, we suggest the use of the SDS model for re-examining the findings of Rose and Fortune from a theoretical perspective, with a particular emphasis on clarifying the effect of both passive and active properties of the dendrite on filtering. The SDS model incorporates passive membrane properties within the cable and mimics active properties by the IF process in the spine-head. Importantly, we have the ability to vary spine distributions and see the effect on filtering. A limitation of the model is that no explicit consideration is given to the dynamics in the soma. However, output signal recordings at the soma in experiments

are believed to be primarily influenced by the spread of activity in the dendrites, suggesting that an analysis of filtering within the SDS model will still be relevant.

We assume that an electrical signal in the form of a periodic pulse train is applied to the dendritic cable at position  $x_0$ . This is modeled by adding the following term to the right-hand side of equation (4)

$$I_{\text{stim}} = \sum_p \delta(x - x_0) \delta(t - pT), \quad (14)$$

where  $T$  is the period of the stimulus. By solving equation (4) with this applied current, we obtain an extra term that enters the right hand side of equation (8) for the membrane potential as follows

$$\sum_{p=0}^P G(x - x_0, t - pT), \quad (15)$$

where  $P = \max\{p \mid t - pT \geq 0\}$ . Therefore, equation (9) for the spines has to be updated accordingly by adding an extra term

$$\frac{1}{r\widehat{C}} \sum_{p=0}^P \widehat{G}(x_n - x_0, t - pT), \quad (16)$$

where  $\widehat{G}(x, t)$  is found as

$$\widehat{G}(x, t) = \int_0^t G(x, s) e^{\varepsilon_0(s-t)} ds = e^{-\varepsilon_0 t} (A_{\varepsilon-\varepsilon_0}(x, 0) - A_{\varepsilon-\varepsilon_0}(x, t)). \quad (17)$$

In Figure 10 we plot the results of simulations of the SDS model driven by the applied forcing signal (14). In all simulations the distribution of spines is chosen to be regular and the current is applied to the left end of the cable at a distance of 0.5 (in units of  $\lambda$ ) from the first spine. In each of these three examples we stimulated the system with a different fixed frequency. Differing applied stimuli lead to different patterns of waves propagating through the system. The signal transformation during its propagation is best established by comparing the applied stimulus and the system response at the opposite end of the cable. Plots on the right in Figure 10 show the membrane voltage at the location of the 55th spine along the cable. If the period of stimulation is large, the signal measured at the end of the cable has a single inter-spike interval (ISI) consistent with the period of stimulus (see Figure 10A). If we decrease the period of stimulation making it closer to the refractory time  $\tau_R$  the output response at the end of the cable shows the presence of two ISIs (in Figure 10B). When the period

of applied current is chosen to be small (Figure 10C), the refractoriness of the system prevents the output from reaching the frequency of the stimulus. Instead, the system initiates repetitive waves consistent with the refractory time, with a single ISI.

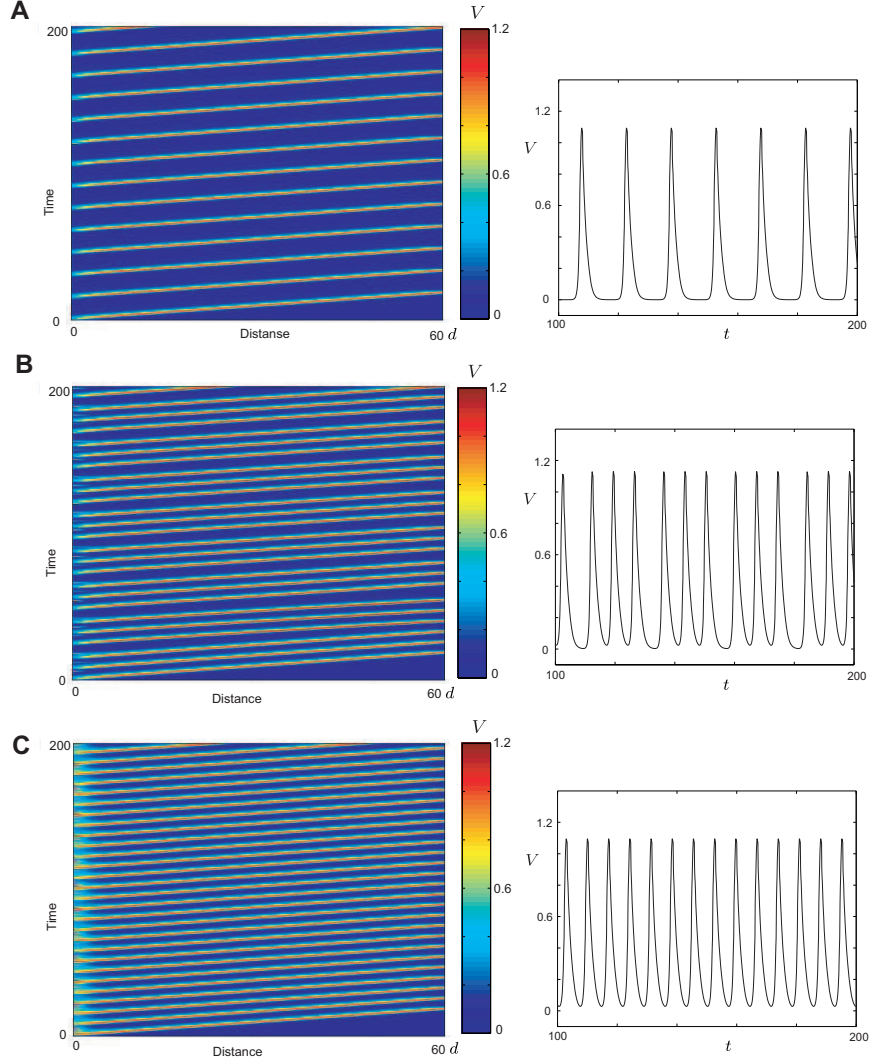


*Figure 10.* Examples of wave propagation in the SDS model driven by periodic stimulation. The current stimulus is applied to the left end of the cable embedded with 60 regularly spaced spines. The system parameters as in Figure 2 with  $d = 0.4$ , except  $\tau_R = 7$ . The period of stimulation is  $T = 15$  (A),  $T = 6$  (B) and  $T = 1$  (C). Plots on the right are examples of voltage profile at the location of the 55th spine along the cable.



The observed correlation between the periods of the applied signal and the ISIs of the system responses is quantified in Figure 11. The  $x$ -axis of the plots in this figure contains the frequencies of the applied stimulus used in the simulations. Along the  $y$ -axis we plot the frequencies at the end of the cable measured as the number of spikes emitted per unit time. Figure 11A shows the data from simulations for a spine spacing with  $d = 0.4$ . Vertical dashed lines in this figure indicate the frequencies of the applied signal used in simulations in Figure 10. The two values for the spike frequencies that are defined for the particular range of input frequencies illustrate the presence of two distinct ISIs, as for example in Figure 10B. The response of the system coincides with the input signal for low frequencies of stimulation, whereas for high frequencies it is limited by the system refractoriness. These dynamics indicate that the SDS model exhibits low-pass temporal filtering properties. The doubly periodic ISIs occur at stimulus periods close to the refractory time-scale. The smaller the distance between the spines, the smaller the range of input frequencies that lead to doubly periodic ISIs. However, if the spines are further apart, the regime of stimulus frequencies where the system responds irregularly with doubly periodic ISIs is increased. An example is shown in Figure 11B, where the spine spacing  $d$  equals 0.8. Thus, the low-pass filtering properties are reduced with decreasing spine density.

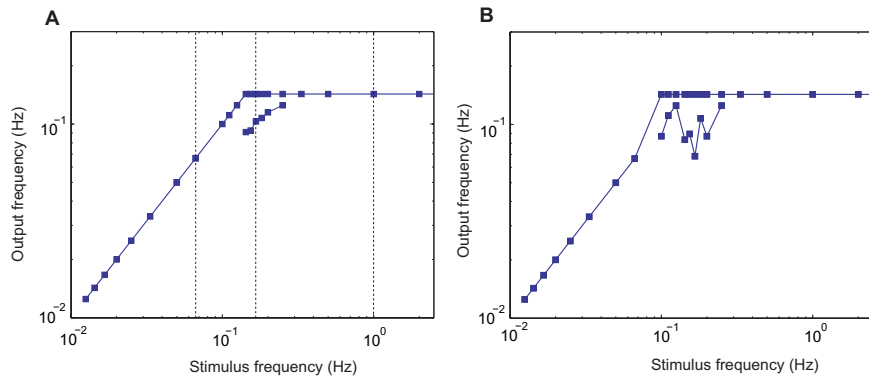


*Figure 11.* Frequency of the applied stimulation vs frequency of spikes in the output response at the end of the cable. The system parameters as in Figure 10 with  $d = 0.4$  in A and  $d = 0.8$  in B. Vertical dashed lines in A indicate the frequencies of stimulation that were chosen for simulations in Figure 10.

In Figure 12 we show the relative amplitude of voltage responses to the frequency of input current. This figure is included to make a link to the experimental observations that spiny neurons demonstrate a decline in the amplitude of voltage responses with increasing stimulation

frequency. The relative amplitude measured in dB is evaluated as the difference between the maximum amplitude and the mean of the signal response. Figure 12A is plotted for two different spine spacings  $d$ . A decrease in the spine density (achieved by increasing  $d$ ) reduces the decline in the voltage amplitude. The presence of doubly periodic ISIs in the voltage response causes the irregularities seen in both curves at periods around the refractory time-scale. In Figure 12B we show that a change in the refractory time in the system results in a shift of the original curve but does not affect the overall trend.

To summarize, the filtering properties of the SDS model are entirely consistent with the experimental observations of Rose and Fortune (Fortune and Rose, 1997; Rose and Fortune, 1999), namely that spiny dendrites with active membrane properties demonstrate low-pass temporal filtering properties.

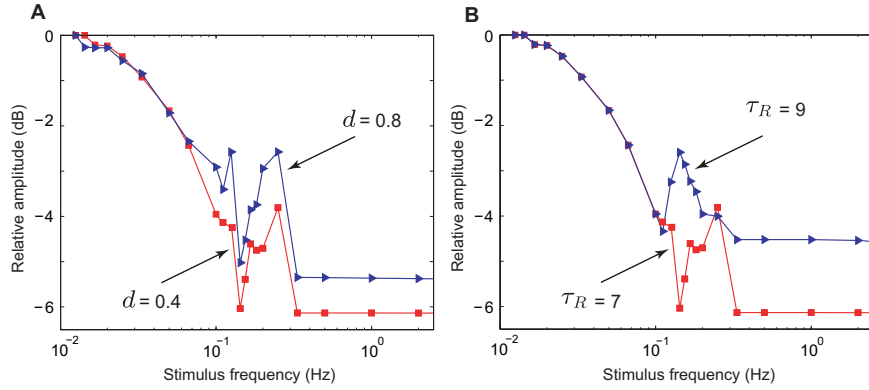


Figure 12. Frequency of applied stimulation vs relative amplitude of the voltage potential (in dB) with the system parameters as in Figure 10. A:  $d = 0.4$  (squares),  $d = 0.8$  (triangles),  $\tau_R = 7$ . B:  $\tau_R = 7$  (squares),  $\tau_R = 9$  (triangles),  $d = 0.4$ .

## 5. Noise induced phenomenon

The spontaneous behavior of neurons *in vivo* is believed to be driven by voltage fluctuations arising from system noise. Such noise can be characterized as either intrinsic or extrinsic. A major source of intrinsic noise arises from the stochastic gating of ion channels in the cell membrane. Importantly, if the membrane potential is close to threshold, channel noise can be critical for the generation of action potentials. In the SDS model the description of noise due to stochastic channels is best introduced in the excitable spine-heads. However, since the

kinetics of ion channels are not explicitly included in the model, the noise is simply considered to lead to the stochastic generation of action potentials. Extrinsic noise sources in the neuron typically arise from synaptic inputs. Interestingly, there is an observed difference between the spontaneous activity of neurons *in vivo* and the activity during intracellular stimulation *in vitro*. Introducing a voltage fluctuation in the cable membrane as well as in the spines is a natural way to mimic the presence of input noise in the SDS model of an isolated neuron.

To study the effects of both types of noise on the properties of wave propagation in the SDS framework we assume that the system is driven by additive white noise in time that is either smooth (correlated) or white (uncorrelated) in space. The SDS model that includes noise both in the cable and the spine-head is given by

$$dV = \left[ D \frac{\partial^2 V}{\partial x^2} - \frac{V}{\tau} + Dr_a \rho(x) \frac{\hat{V} - V}{r} \right] dt + \mu_V dW_V(t, x), \quad (18)$$

$$dU_n = \left[ \frac{V_n}{\bar{C}r} - \varepsilon_0 U_n - h \sum_m \delta(t - T_n^m) \right] dt + \mu_U dW_U(t, x). \quad (19)$$

This is in fact a system of integral equations where we interpret noise in the Itô sense. We assume that the Wiener processes  $W_{V,U}$  are of the form

$$W(t, x) = \sum_{n \in \mathbb{Z}} b_n \phi_n \beta_n(t),$$

where the  $\beta_n$  are a mutually independent ordinary set of Brownian motions and the  $\phi_n$  are appropriate basis functions (with either periodic or Neumann boundary conditions). The coefficients  $b_n$  determine the spatial correlation. For spatially correlated noise we take

$$\sum_{n \in \mathbb{Z}} e^{2\alpha|n|} |b_n|^2 < \infty.$$

Here, the parameter  $\alpha$  determines the correlation length scale and the spatial smoothness. Examples of such noise are considered for example in (Da Prato and Zabczyk, 1992; Shardlow, 2005; García-Ojalvo and Sancho, 1999; Lord and Rougemont, 2004). The parameters  $\mu_V$  and  $\mu_U$  describe the strength of the noise in the cable and in the spine-head respectively.

The integration of equation (18) for the membrane potential leads to a solution for  $V(x, t)$  that may be split into two terms. The first term, representing the deterministic component, may be computed using the exact solution given by equation (8), whereas the second term incorporating the noise has to be evaluated numerically. To evaluate this term we enforce a spatial correlation in Fourier space and use a Brownian

increment of mean zero and finite variance in time, as discussed for example in (Kloeden and Platen, 1992). The noise for an infinite cable was approximated by applying periodic boundary conditions of twice the numerical cable length and taking the central portion away from the boundary. The integration of equation (19) for  $U_n(t)$ , similarly to the cable, generates two terms. In general, the first term has to be evaluated numerically and we use an explicit Euler-Maruyama method of approximation. The second term, that defines the noise in the spine-head, was generated in the same manner as for the cable and then sampled at the spine position. However, when  $\mu_V = 0$ , the model reduces to the case where only the spines are forced by noise and, thus, the solution for  $V(x, t)$  is explicitly defined. In this limit, the numerical evaluation of the first term in the solution of equation (19) can be avoided. Instead, this term is found using the explicit equation (9).

Here we demonstrate the effect noise can have on the properties of wave propagation in the SDS model. We begin by exploring the SDS model with noise only in the spine-head and take  $\mu_V = 0$ . In all of the figures that follow the noise-path is the same and  $\mu_U$  is the only parameter that varies. In all simulations the spines are regularly distributed along the cable. When  $d = 0.6$  (left of LP in 2) there is propagation in the absence of noise as illustrated in Figure 13. In general, by increasing the level of noise in the system the patterns of cell response change from isolated or repetitive wave propagation to the case of almost simultaneous firing of all spines (i.e., a coherent behavior). However, as shown in Figures 13A and B, at low noise levels the repetitive propagation of waves can be suppressed by a small noise increase. For high noise (Figure 13D) the majority of spines can generate an action potential immediately and this leads to the activation of residual spines (i.e., those that did not fire) shortly thereafter. When  $d = 1$  (right of LP in 2) the system does not support traveling waves in the absence of noise. However, the examples in Figure 14 illustrate that it is possible for noise to sustain spatio-temporal structures that could not otherwise occur. In particular, for a low level of noise we observe purely noise induced waves such as shown in Figure 14A. Propagation failure occurs if the level of noise is below some critical value. In regions of high noise it is possible to see coherent oscillations in the system (Figure 14B) where almost all spines simultaneously generate action potentials. Choosing correlated noise in the spine-head instead of white noise does not yield a qualitative change in system behavior. This is illustrated in Figure 15 where we plot two examples of spatio-temporal structures generated by correlated noise. The patterns of wave propagation are similar to the examples shown in Figure 14.

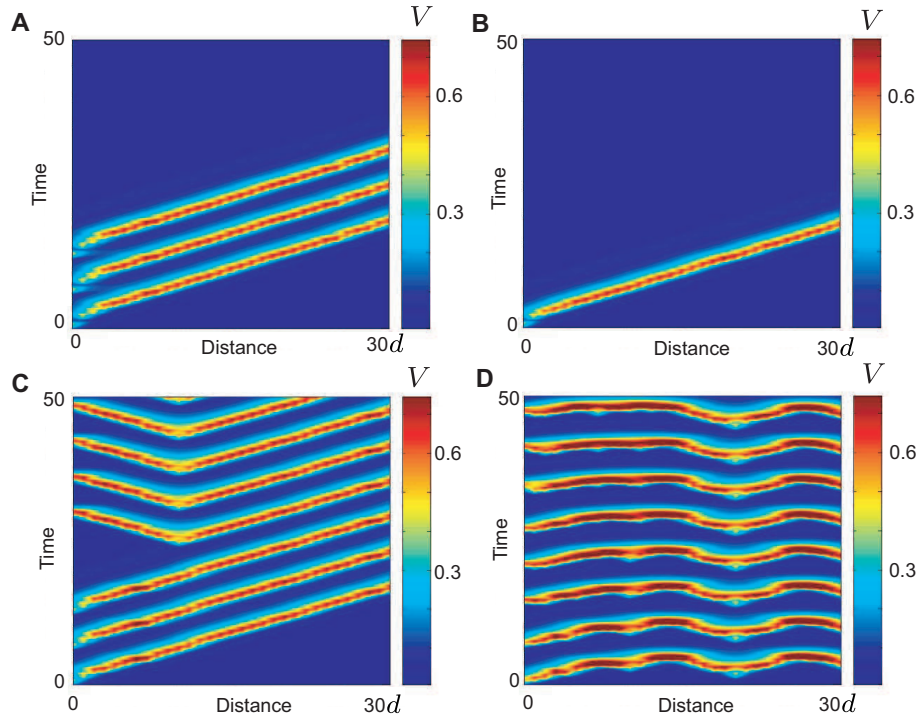


Figure 13. Traveling waves in the SDS model in the presence of uncorrelated white noise in the spine-heads for parameters  $d = 0.6$ ,  $\mu_V = 0$  and A:  $\mu_U = 0.007$ , B:  $\mu_U = 0.009$ , C:  $\mu_U = 0.015$ , D:  $\mu_U = 0.028$ . Other parameters as in Figure 7

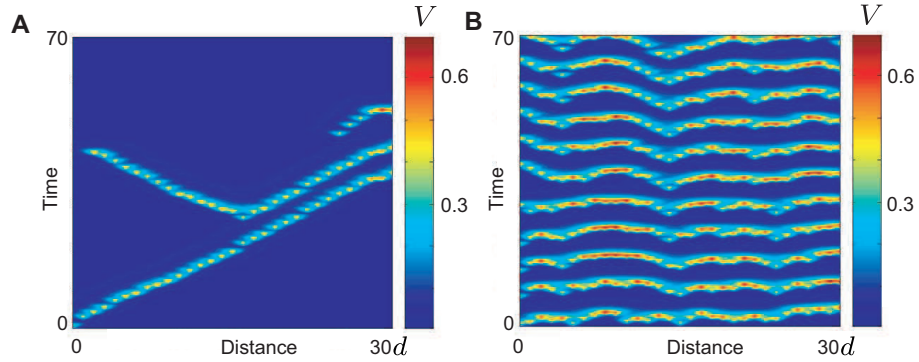


Figure 14. Traveling waves in the SDS model in the presence of uncorrelated white noise in the spine-heads for parameters  $d = 1$ ,  $\mu_V = 0$  and A:  $\mu_U = 0.03$ , B:  $\mu_U = 0.055$ . Other parameters as in Figure 7.

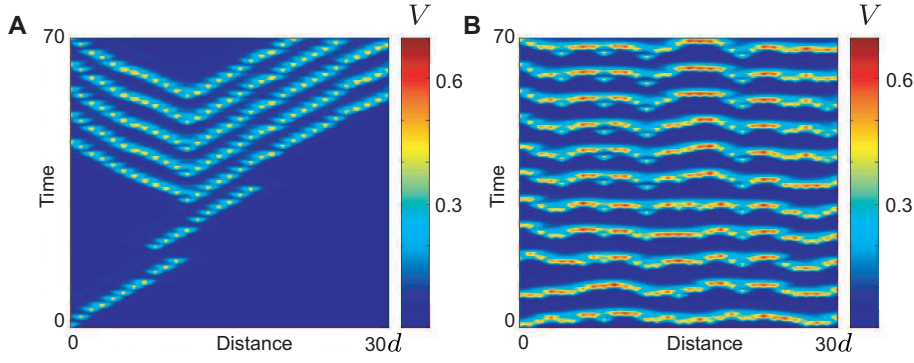


Figure 15. Traveling waves in the SDS model in the presence of correlated noise in the spine-heads for the parameters  $\alpha = 1$ ,  $d = 1$ ,  $\mu_V = 0$  and A:  $\mu_U = 0.17$ , B:  $\mu_U = 0.4$ . Other parameters as in Figure 7.

The noise term in equation (19) for the spine-heads dynamics leads to a stochastic process for spike generation. Another way to incorporate this stochasticity into the firing events is to introduce a source of noise at the threshold level. This can be modeled under the replacement  $h \rightarrow h + \xi$  where  $\xi$  is an additive noise with distribution  $\rho(\xi)$ . This approach can be simply implemented by generating a random vector  $\xi$  of length  $n$  from a distribution of mean  $h$  and standard deviation  $\beta$  at each small time step. Then the firing events are defined by checking the threshold conditions  $U_n > \xi_n$  where  $\xi_n$  is the  $n$ th element of vector  $\xi$  and  $U_n$  is given by equation (9). The level of noise in the system is controlled by the parameter  $\beta$ . The numerical simulations of the SDS model in the presence of threshold noise demonstrate consistency with the results of the model driven by the stochastic forcing at the spine-heads. It is also possible to model the effect of threshold noise using a probabilistic rule for spike generation. To see this we consider drawing the threshold noise from a distribution  $\sigma$ , so that the probability of a firing event can be written

$$P(U_n > h) = \int \sigma(\xi) \Theta(U_n - h - \xi) d\xi = f(U_n - h), \quad (20)$$

where  $f(\xi) = \int^\xi \sigma(x) dx$ . Considering a bell-shaped noise distribution for  $\sigma$ , then the function  $f$  will have a sigmoidal shape. Here we use the following form for the function  $f$

$$f(U) = (1 + e^{-\gamma h}) / (1 + e^{-\gamma U}) - e^{-\gamma h}, \quad (21)$$

so that the probability of a firing event is zero and one respectively for  $U = 0$  and  $U \rightarrow \infty$ . The parameter  $\gamma$  in (21) controls the level

of noise in the system by determining the width of the bell-shaped distribution  $\sigma$  (such that decreasing  $\gamma$  corresponds to increasing noise). Simulation results of the SDS model with this probabilistic update rule are shown in Figure 16. Plots on the left are for the system with spine spacing  $d = 0.6$ , whereas plots on the right are obtained when  $d = 1$ . For low noise the system is able to support repetitive wave propagation as illustrated in Figures 16A and D. When the noise level is below some critical value, propagation failure occurs. This is similar to the behavior observed in our earlier examples of the stochastic SDS model. Here, however, an increase in noise causes more irregularity in the patterns of wave propagation (see Figures 16B and E). Moreover, high noise limits the spread of activity in the system by inhibiting wave propagation (see Figures 16C and F) or can even lead to propagation failure. The probabilistic rule used for the determination of the spikes in these last examples ensures that the probability of an individual spine being fired is low if the membrane voltage in the cable at the location of this spine is low. This explains why wave propagation can terminate for high noise levels. In previous examples, where the noise in the spines is modeled by the stochastic differential equation (19), the high noise in the system, contrary to this last example, stimulates activity along the whole cable.

Now consider the stochastic SDS model driven by noise in the cable and thus, take  $\mu_U = 0$ . In Figure 17 we plot results of simulations for the system in the presence of uncorrelated white noise. These examples demonstrate that in the parameter region where waves propagate in the absence of noise ( $d = 0.6$ ), an increase in noise level can lead to repetitive wave initiation. Plots on the right show profiles of action potentials in the membrane at the locations of the 20th and 12th spine along the cable (Figures 17A and B). In the presence of correlated rather than white noise, the system demonstrates a similar kind of behavior. This is shown in Figure 18 where increasing noise levels generate a single, double and repetitive wave respectively.

If the distance between the spines is chosen to be large, the noise in the cable, white or correlated, is not able to initiate any wave propagation in the system. However, in the case of high white noise some limited activity might be possible. An example is illustrated in Figure 19. The plot on the right shows the firing times of spines that generated action potentials during the simulation.

In summary, from our numerical simulation studies we conclude that noise in the spine-heads has a strong effect on the properties of wave propagation. In the parameter regime where the deterministic model fails to support waves, noise in the spines may aid in the initiation and propagation of waves. Moreover, for high noise in the spines one

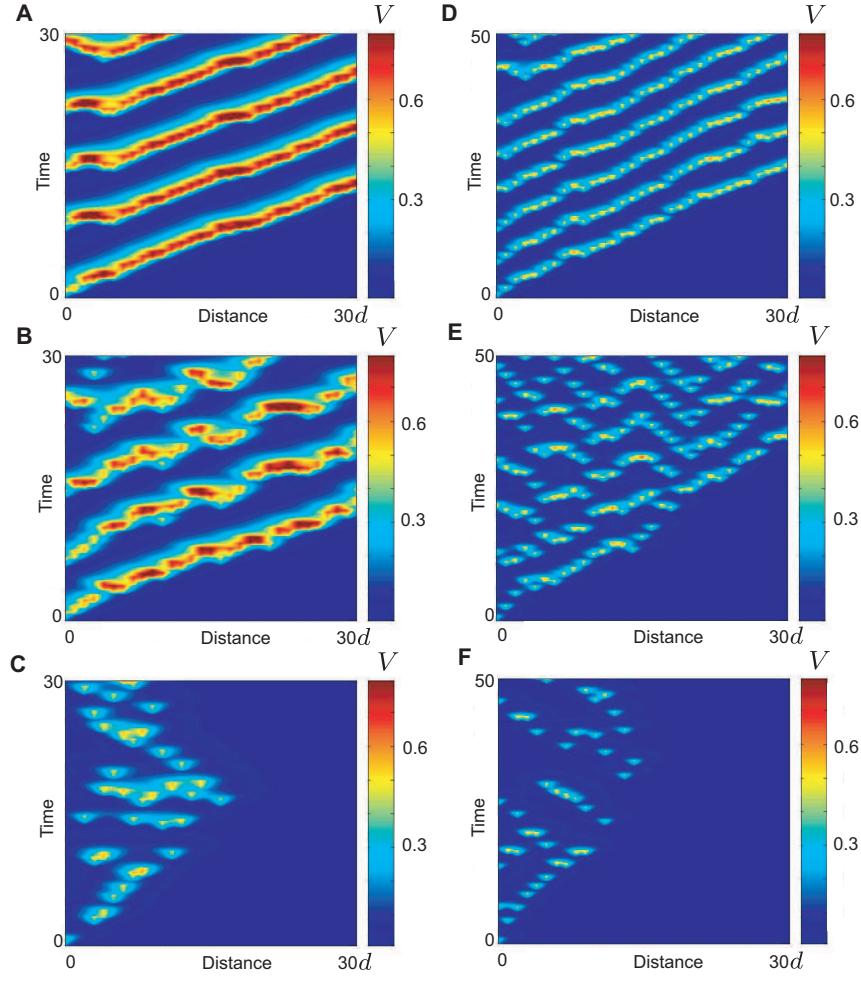


*Figure 16.* Traveling waves in the SDS model in the presence of threshold noise incorporated by the probabilistic rule for the spine spacing  $d = 0.6$  (A, B and C) and  $d = 1$  (D, E and F). The noise levels are  $\gamma = 60$  (low noise) (A and D),  $\gamma = 5$  (medium noise) (B and E),  $\gamma = 0.8$  (C) and  $\gamma = 1$  (high noise) (F). Other parameters as in Figure 7.

observes coherent oscillations. At the same time, the stochastic SDS model shows robustness of wave propagation to low noise in the spine-heads. On the other hand, noise in the cable does not have a strong effect on patterns of activity.

We now consider the presence of noise both in the cable and in the spine-heads (see Figure 20). Noise in the cable was chosen as for the model in Figure 18B. For Figure 20A (Figure 20B) noise in the



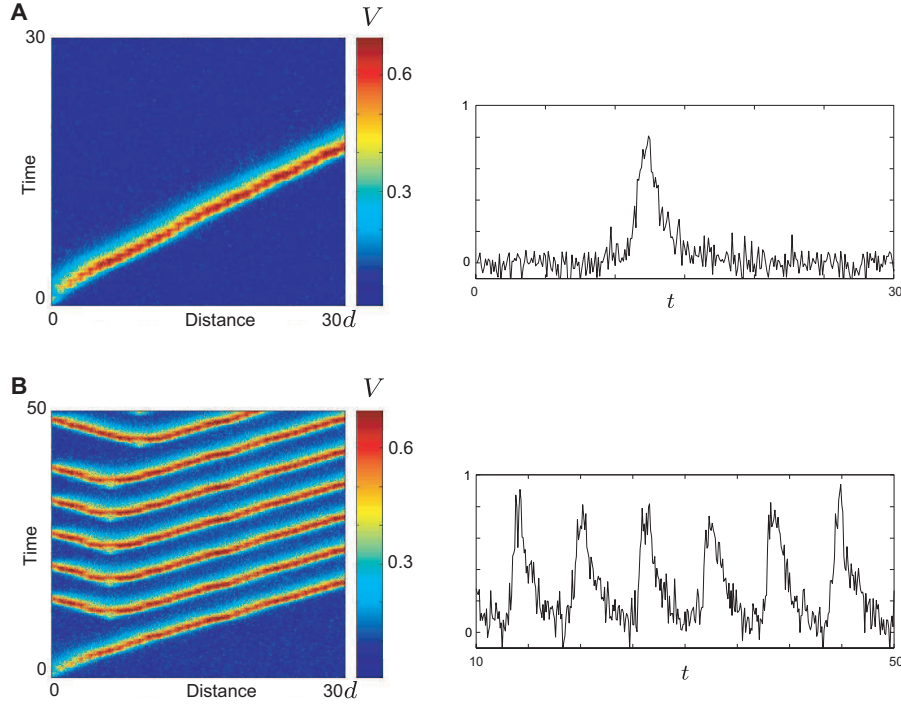


Figure 17. Traveling waves in the SDS model in the presence of uncorrelated white noise in the cable for the parameters  $d = 0.6$ ,  $\mu_U = 0$  and A:  $\mu_V = 0.08$ , B:  $\mu_V = 0.114$ . Other parameters as in Figure 7. Plots on the right show the profiles of membrane voltage at the locations of 20th (A) and 12th spine (B) along the cable.

spine-heads was generated as in Figure 13B (Figure 14A). Simulations demonstrate that in the parameter regime where the reduction of noise to zero would still support wave propagation the cable noise stimulates the repetitive initiation of waves (see Figure 20A).

Finally, we investigate the robustness of the filtering properties observed in the deterministic SDS model to noise sources. The SDS model in the presence of a small amount of correlated noise both in the cable and the spine-heads was driven by injected current in the form of a periodic pulse train as in section 4. In Figure 21 we demonstrate examples of membrane voltage profiles along the cable for three different periods of stimulation. These plots should be compared with the results of simulations shown in Figure 10. The presence of noise in the system for the low and high periods of stimulation (Figures 21A and C) retains the same ISIs as in the deterministic model. When the period of stimulation is close to the refractory time the well-defined pattern of doubly periodic ISIs seen in Figure 10B can be destroyed by noise.

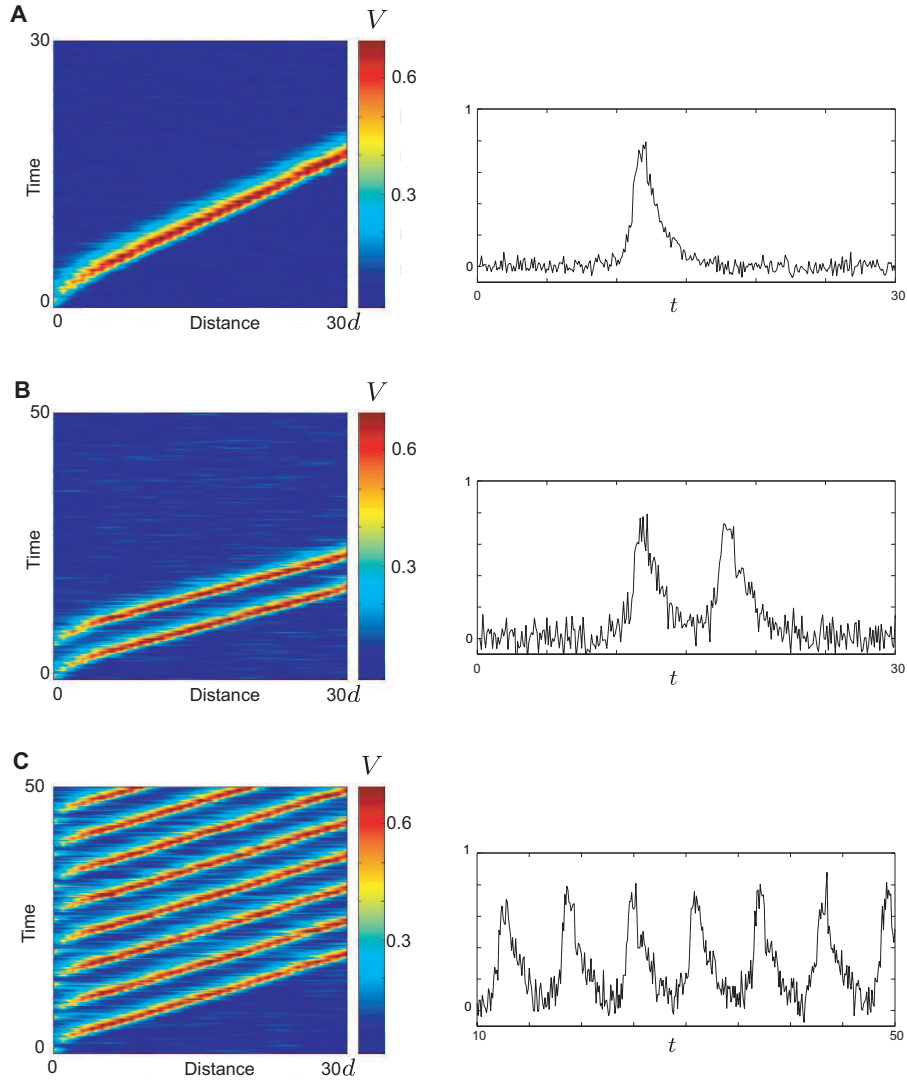


Figure 18. Traveling waves in the SDS model in the presence of correlated noise in the cable for the parameters  $\alpha = 1$ ,  $d = 0.6$ ,  $\mu_U = 0$  and A:  $\mu_V = 0.4$ , B:  $\mu_V = 0.8$  and C:  $\mu_V = 0.81$ . Other parameters as in Figure 7. Plots on the right show the profiles of membrane voltage at the locations of 20th spine along the cable.

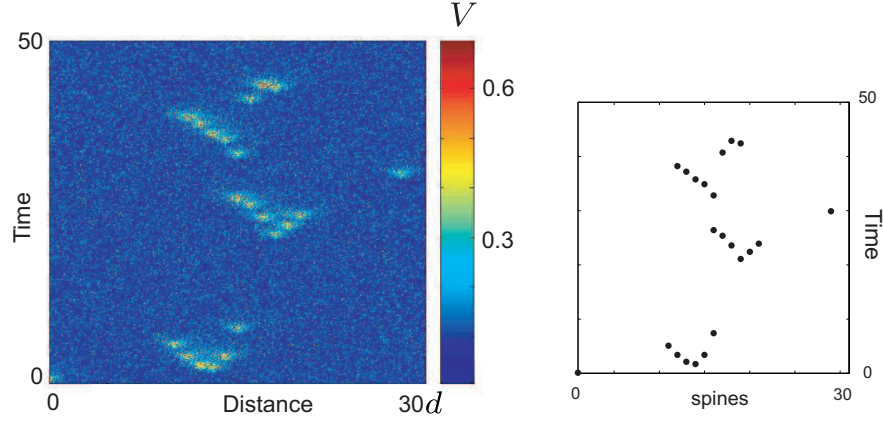


Figure 19. Traveling waves in the SDS model in the presence of uncorrelated white noise in the cable for the parameters  $d = 1$ ,  $\mu_U = 0$  and  $\mu_V = 0.35$ . Other parameters as in Figure 7. Plot on the right shows the spines that generate the action potential.

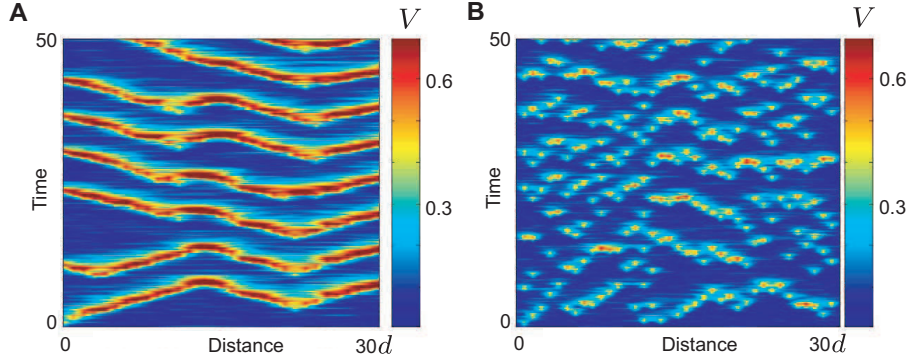


Figure 20. Traveling waves in the SDS model in the presence of uncorrelated white noise in the spines-heads and correlated noise in the cable for the parameters A:  $d = 0.6$ ,  $\alpha = 1$ ,  $\mu_V = 0.8$ ,  $\mu_U = 0.009$  and B:  $d = 1$ ,  $\alpha = 1$ ,  $\mu_V = 0.8$ ,  $\mu_U = 0.03$ . Other parameters as in Figure 7.

However, in general the low-pass temporal filtering properties observed in the deterministic model are robust to noise.

## 6. Discussion

It is now just over one hundred years since the discovery of spines, yet there are still mysteries about the contribution they make to single neuron dynamics. Building on the insight into dendritic function gained

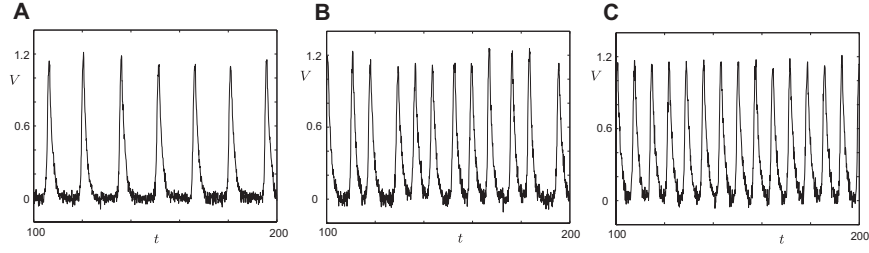


Figure 21. Examples of voltage profiles at the location of the 55th spine along the cable in the stochastic SDS model driven by the applied current stimulation of period  $T$ . The parameters are  $\alpha = 0.4$ ,  $\mu_V = 0.49$ ,  $\mu_U = 0.043$  and  $T = 15$  (A),  $T = 6$  (B) and  $T = 1$  (C). Other system parameters as in Figure 10.

since the pioneering theoretical work of Rall in the 1950's (surveyed in (Segev et al., 1995)), we propose that the SDS model is ideally suited to probing how active spines shape and modulate a spatially structured input. In this paper we have focused on a rather simple (spatially localized) input, though we emphasize here that more spatially structured input can also be treated. Moreover, there is no barrier to working with a truly branched dendritic tree model as the analytical ("sum-over-paths") techniques necessary to do this have already been developed by Bressloff et. al. (1996). In future work we propose to use the SDS model to understand whether inputs to a neuron sum linearly, or depend on spatial relationships in the input, such as clustering. The currently available experimental evidence is conflicting (Cash and Yuste, 1998; Polsky et al., 2004). Interestingly, recent advances in imaging technology (using fluorescent dyes in combination with confocal or two-photon laser scanning microscopy) have permitted time-lapse observation of spine morphology in living neurons (Fischer et al., 1998; Dunaevsky et al., 1999; Bonhoeffer and Yuste, 2002), showing that spines are also constantly moving. In fact over time-scales of seconds, spines continuously undergo small changes in shape, thought to be powered by dynamic actin filaments. On timescales of minutes to hours spines can change their shape dramatically or even appear or disappear. Moreover, new spines can be generated in response to synaptic stimulation that also results in strengthening of synapses. These morphological changes could underlie some of the changes in synaptic strength induced by neural activity. Working within the SDS framework we would also be in a position to examine how successive synaptic input might influence spine motility and electro-chemical properties. Some work in this direction has already been done by Verzi et. al. (2005), for the continuum Baer and Rinzel model using phenomenological models of spine density dynamics. Within the SDS framework we envisage

complementary work, building on existing modeling studies (of spines as calcium compartments) such as that of Holcman and Schuss (2005), exploring how calcium accumulates in discrete spines, and how this makes its way to the cell nucleus and triggers genetic mechanisms that ultimately lead to the mechanical reconfiguration of the synapse. Both the above issues are topics of current investigation and will be reported upon elsewhere.

### Acknowledgments

We would like to thank Steve Cox, Krešimir Josić and Costa Colbert for useful discussions about potential applications of the SDS model. The work in this paper is supported through EPSRC Grant No. GR/S60914/01. SC would also like to acknowledge ongoing support from the EPSRC through the award of an Advanced Research Fellowship, Grant No. GR/R76219.

### Appendix A: $A_\varepsilon(x, t)$

$$A_\varepsilon(x, t) = \frac{\eta_0}{4} \sqrt{\frac{1}{\varepsilon D}} \left\{ \exp\left(-|x| \sqrt{\frac{\varepsilon}{D}}\right) \operatorname{erfc}\left(-\frac{|x|}{\sqrt{4Dt}} + \sqrt{\varepsilon t}\right) + \exp\left(|x| \sqrt{\frac{\varepsilon}{D}}\right) \operatorname{erfc}\left(\frac{|x|}{\sqrt{4Dt}} + \sqrt{\varepsilon t}\right) \right\}.$$

### Appendix B: Equations of the BR model

$$\begin{aligned} I(\hat{V}, m, n, h) &= g_K n^4 (\hat{V} - v_K) + g_{Na} h m^3 (\hat{V} - V_{Na}) + g_L (\hat{V} - V_L), \\ \tau_X(\hat{V}) \frac{dX}{dt} &= X_\infty(\hat{V}) - X, \end{aligned}$$

for  $X \in \{m, n, h\}$  where  $V_L$ ,  $V_K$  and  $g_{Na}$  represent the constant membrane reversal potentials associated with the leakage, potassium and sodium channels respectively.

$$\tau_X(\hat{V}) = \frac{1}{\alpha_X(\hat{V}) + \beta_X(\hat{V})},$$

$$X_\infty(\hat{V}) = \alpha_X(\hat{V})\tau_X(\hat{V}),$$

where

$$\alpha_m(\hat{V}) = \frac{0.1(\hat{V} + 40)}{1 - \exp[-0.1(\hat{V} + 40)]},$$

$$\alpha_h(\hat{V}) = 0.07\exp[-0.05(\hat{V} + 65)],$$

$$\alpha_n(\hat{V}) = \frac{0.01(\hat{V} + 55)}{1 - \exp[-0.1(\hat{V} + 55)]},$$

$$\beta_m(\hat{V}) = 4.0\exp[-0.0556(\hat{V} + 65)],$$

$$\beta_h(\hat{V}) = \frac{1}{1 + \exp[-0.1(\hat{V} + 35)]},$$

$$\beta_n(\hat{V}) = 0.125\exp[-0.0125(\hat{V} + 65)].$$

The following parameter values were used:  $R_a = 36 \text{ } \Omega \cdot \text{cm}$ ,  $R_m = 3333 \text{ } \Omega \cdot \text{cm}^2$ ,  $C_m = 1 \text{ } \mu\text{F}/\text{cm}^2$ ,  $a = 1 \text{ } \mu\text{m}$ ,  $r = 0.05 \text{ M}\Omega$ ,  $\hat{C} = 0.001 \text{ } \mu\text{F}$ ,  $g_L = 0.0003 \text{ mS}$ ,  $g_K = 0.036 \text{ mS}$ ,  $g_{Na} = 0.12 \text{ mS}$ ,  $V_L = -54.402 \text{ mV}$ ,  $V_K = -77 \text{ mV}$  and  $V_{Na} = 50 \text{ mV}$ .

## References

- Baer, S. M. and J. Rinzel: 1991, ‘Propagation of dendritic spikes mediated by excitable spines: A continuum theory’. *Journal of Neurophysiology* **65**(4), 874–890.
- Bonhoeffer, T. and R. Yuste: 2002, ‘Spine motility: phenomenology, mechanisms and function’. *Neuron* **35**, 1019–1027.
- Bressloff, P. C. and S. Coombes: 1997, ‘Physics of the extended neuron’. *International Journal of Modern Physics B* **11**, 2343–2392.
- Bressloff, P. C., V. M. Dwyer, and M. J. Kearney: 1996, ‘Sum-over-paths approach to diffusion on trees’. *Journal of Physics A* **29**, 1881–1896.
- Cajal, R.: 1891, ‘Significación fisiológica de las expansiones protoplásmicas y nerviosas de la sustancia gris’. *Revista de ciencias mde Barcelona* **22**, 23.
- Cajal, R.: 1899, ‘Estudios sobre la corteza cerebral humana: corteza visual’. *Rev. Trim. Microgr.* **4**, 1–63.
- Cash, S. and R. Yuste: 1998, ‘Input summation by cultured pyramidal neurons is linear and position independent’. *Journal of Neuroscience* **18**, 10–15.

- Coombes, S.: 2001a, 'The effect of ion pumps on the speed of travelling waves in the fire-diffuse-fire model of  $\text{Ca}^{2+}$  release'. *Bulletin of Mathematical Biology* **63**, 1–20.
- Coombes, S.: 2001b, 'From periodic travelling waves to travelling fronts in the spike-diffuse-spike model of dendritic waves'. *Mathematical Biosciences* **170**, 155–172.
- Coombes, S. and P. C. Bressloff: 2000, 'Solitary waves in a model of dendritic cable with active spines'. *SIAM Journal on Applied Mathematics* **61**, 432–453.
- Coombes, S. and P. C. Bressloff: 2003, 'Saltatory waves in the spike-diffuse-spike model of active dendritic spines'. *Physical Review Letters* **91**, 028102.
- Da Prato, G. and J. Zabczyk: 1992, *Stochastic Equations in Infinite Dimensions*, Vol. 44 of *Encyclopedia of Mathematics and its Applications*. Cambridge University Press.
- Dunaevsky, A., A. Tashiro, A. Majewska, C. Mason, and R. Yuste: 1999, 'Developmental regulation of spine motility in mammalian CNS'. *Proceedings of the National Academy of Sciences USA* **96**(23), 13438–13443.
- Fischer, M., S. Kaech, D. Knutti, and A. Matus: 1998, 'Rapid actin-based plasticity in dendritic spine'. *Neuron* **20**(5), 847–854.
- Fortune, E. S. and G. J. Rose: 1997, 'Passive and active membrane properties contribute to the temporal filtering properties of midbrain neurons *In Vivo*'. *The Journal of Neuroscience* **17**, 3815–3825.
- García-Ojalvo, J. and J. M. Sancho: 1999, *Noise in Spatially Extended Systems*. Springer.
- Hines, M. L. and N. T. Carnevale: 2003, *The Handbook of Brain Theory and Neural Networks*, Chapt. The NEURON simulation environment, pp. 769–773. Cambridge, MA: MIT Press.
- Holcman, D. and Z. Schuss: 2005, 'Modeling calcium dynamics in dendritic spines'. *SIAM Journal on Applied Mathematics* **65**(3), 1006–1026.
- Jack, J. J. B., D. Noble, and R. W. Tsien: 1975, *Electric Current Flow in Excitable Cells*. Clarendon Press.
- Kloeden, P. E. and E. Platen: 1992, *Numerical solution of stochastic differential equations*, Vol. 23 of *Applications of Mathematics*. Springer-Verlag.
- Larkum, M. E., J. J. Zhu, and B. Sakmann: 1999, 'A new cellular mechanism for coupling inputs arriving at different cortical layers'. *Nature* **398**, 338–341.
- Lord, G. J. and S. Coombes: 2002, 'Traveling waves in the Baer and Rinzel model of spine studded dendritic tissue'. *Physica D* **161**, 1–20.
- Lord, G. J. and J. Rougemont: 2004, 'A numerical scheme for stochastic PDEs with Gevrey regularity'. *IMA Journal on Numerical Analysis* **24**, 587–604.
- Mel, B. W., D. L. Ruderman, and K. A. Archie: 1998, 'Translation-invariant orientation tuning in visual 'complex' cells could derive from intradendritic computations'. *The Journal of Neuroscience* **18**, 4325–4334.
- Miller, J. P., W. Rall, and J. Rinzel: 1985, 'Synaptic amplification by active membrane in dendritic spines'. *Brain Research* **325**, 325–330.
- Polsky, A., B. W. Mel, and J. Schiller: 2004, 'Computational subunits in thin dendrites of pyramidal cells'. *Nature Neuroscience* **7**(6), 621–627.
- Rose, G. J. and E. S. Fortune: 1996, 'New techniques for making whole-cell recordings from CNS neurons *In Vivo*'. *Neuroscience Research* **26**, 89–94.
- Rose, G. J. and E. S. Fortune: 1999, 'Mechanisms for generating temporal filters in the electrosensory system'. *The Journal of Experimental Biology* **202**, 1281–1289.
- Segev, I. and W. Rall: 1998, 'Excitable dendrites and spines: earlier theoretical insights elucidate recent direct observations'. *Trends in Neuroscience* **21**(11), 453–460.

- Segev, I., J. Rinzel, and G. M. Shepherd (eds.): 1995, *The theoretical foundations of dendritic function: selected papers of Wilfrid Rall with commentaries*. MIT Press.
- Shardlow, T.: 2005, 'Numerical simulation of stochastic PDEs for excitable media'. *Journal of Computational and Applied Mathematics* **175**(2), 429–446.
- Shepherd, G. M. and R. K. Brayton: 1987, 'Logic operations are properties of computer-simulated interactions between excitable dendritic spines'. *Neuroscience* **21**(1), 151–165.
- Shepherd, G. M., R. K. Brayton, J. P. Miller, I. Segev, J. Rinzel, and W. Rall: 1985, 'Signal enhancement in distal cortical dendrites by means of interactions between active dendritic spines'. *Proceedings of the National Academy of Sciences USA* **82**, 2192–2195.
- Verzi, D. W., M. B. Rheuben, and S. M. Baer: 2005, 'Impact of time-dependent changes in spine density and spine shape on the in-out properties of a dendritic branch: A computational study'. *Journal of Neurophysiology* **93**, 2073–2089.
- Yuste, R. and T. Bonhoeffer: 2001, 'Morphological changes in dendritic spines associated with long-term synaptic plasticity'. *Annual Review of Neuroscience* **24**, 1071–1089.
- Yuste, R. and A. Majewska: 2001, 'On the function of dendritic spines'. *Neuroscientist* **7**(5), 387–395.
- Zito, K. and V. N. Murthy: 2002, 'Dendritic spines'. *Current Biology* **12**, R5.